Theory of giant magnetoresistance for parallel and perpendicular currents in magnetic multilayers

H. Itoh, J. Inoue, and S. Maekawa
Department of Applied Physics, Nagoya University, Nagoya 464-01, Japan
(Received 18 May 1994)

For a magnetic multilayer system, the physical origin of the difference between the giant magnetoresistances for currents parallel and perpendicular to the layer planes is studied. In order to take into account the two characteristics of a multilayer system, interfacial roughness and layered structure, we adopt the single-cell coherent-potential approximation. The spin-dependent resistivities are calculated for currents parallel and perpendicular to the layer planes by using a single-band tight-binding model and the Kubo formalism. It is shown that the magnetoresistance ratio for perpendicular current is larger than that for parallel current. The difference between magnetoresistances for parallel and perpendicular currents is attributed to the fact that the effects of the anisotropy of the effective mass and the two-dimensional distribution of randomness on the anisotropy of the resistivity depend on the spin-dependent potential. It is also shown that interfacial roughness is favorable to magnetoresistance for parallel currents.

I. INTRODUCTION

Magnetic multilayers have provided novel magnetic and transport phenomena in the field of magnetism: the long range exchange coupling between magnetic layers[1,2] and the giant magnetoresistance (MR). Since the first observation of the giant MR in Fe/Cr multilayers,[3] many investigations of the magnetotransport properties in magnetic multilayers have been stimulated and it has been found that many multilayers such as Co/Cu,[4,5] Co/Cu/NiFe/Cu,[6] Fe-Co/Cu,[7,8] Co-Ni/Cu,[9] Fe-Co-Ni/Cu,[10] etc., show the giant MR. The giant MR is different from the conventional anisotropic MR because the decrease of the resistivity in the giant MR of multilayers is independent of the relative direction of the applied magnetic field and the direction of currents.[11] The electrical resistivity decreases with the reorientation of the magnetization within the magnetic layers from an antiparallel (antiferromagnetic) alignment to a parallel (ferromagnetic) alignment by the magnetic field. With increasing the net magnetization of the system, the resistivity decreases and becomes independent of the magnitude of the field after the saturation of the magnetization. The fact that the resistivity depends on the direction of the magnetization of the magnetic layers indicates that spin-dependent resistivity is responsible for the giant MR. The giant MR is usually measured for currents parallel to the layer planes. Recently, the giant MR for currents perpendicular to the layer planes has been measured and it has been reported that the MR ratio for perpendicular currents ($MR_\perp$) is much larger than that for the parallel currents ($MR_\parallel$).[12–16]

These findings have brought up several important issues to be studied theoretically: (1) the origin of the spin-dependent resistivity, (2) transport properties in layered structures, (3) material dependence of the giant MR, (4) relations between the giant MR and other transport phenomena such as the thermoelectric power, thermal conductivity, and Hall resistivity, (5) temperature dependence of the giant MR, and so on. Several theoretical works on the giant MR have dealt with the electrical resistivity in the layered structures.[17–22] In these theories, however, the asymmetry of the spin-dependent scattering was treated as an adjustable parameter to explain the giant MR observed. In our previous papers,[23–25] we have attributed the origin of the spin-dependent scattering to the randomness of the exchange and atomic potentials caused by interfacial roughness, and have studied the material dependence of the giant MR by calculating the electronic structures near the interfaces. It is natural to consider that the roughness of the interfaces plays an important role in the giant MR when we note that large residual resistivity exists in the multilayers and that the interfaces are the boundaries of magnetic and nonmagnetic layers. The successful explanation of the material dependence of the giant MR by detailed calculations of the electronic structures supports the basic assumptions of our model.[26] The spin-dependent scattering at the interfaces is also supported by experimental fact that the MR depends on the roughness of the interfaces[27,28] and that it changes dramatically when thin layers of a third element are inserted at the interfaces.[29–31] We have further investigated the relation between the giant MR, thermoelectric power, and thermal conductivity and have obtained a basic agreement between the theoretical and experimental results.[32–37] As for the temperature dependence of the giant MR, several explanations have been presented; a dilution effect,[38] spin fluctuation effects,[39] and magnon scattering.[40]

In order to explain the outstanding feature of $MR_\perp$, namely, that it is much larger than $MR_\parallel$, several theoretical frameworks have been developed by using semiclassical[41–45] and quantum theories[46–48] including numerical simulations.[49,50] Possible physical mechanisms

for $MR_\perp \gg MR_\parallel$ have been proposed: effects of backscattering (or vertex correction) on the conductivity, diffuse scattering at the interfaces, and/or miniband structures (or the anisotropy of the effective mass of the electrons). Although these effects clearly make the resistivity of perpendicular currents larger than that of parallel currents, it is not evident that they also make $MR_\perp$ larger than $MR_\parallel$. Thus, the physical origin of the observed results still seems to be far from fully understood. To clarify the physical reasons of $MR_\perp \gg MR_\parallel$, we must take into account the layered structures of the systems and interfacial roughness explicitly and study the dependence of the resistivity on the direction of the currents and on the change in the periodicity due to the alternation of the alignment of the magnetizations by the external magnetic field. The numerical simulation[49,50] based on the Kubo formalism is a powerful method to include these effects because no approximation is made in this method. A shortcoming in this method, however, is the effects of the contact resistance due to the finiteness of the system used in the simulations.

The purpose of this paper is to present a method to study the origin of the difference between $MR_\parallel$ and $MR_\perp$ (Ref. 51) for infinite systems and to provide some implications for the experiments. In this work, the spin-dependent resistivity will be calculated in the Kubo formalism by taking into account the layered structures and the randomness at the interfaces explicitly but some approximations will be made in the treatment of the randomness. The present method and the numerical simulations may be complementary to each other. Although there may be several types of the randomness in multilayers, we confine ourselves to substitutional randomness caused by the interfacial roughness. The structural randomness such as grain boundaries, lattice distortion, lattice defects, etc., is neglected because it may be less important for the spin-dependent scattering. In the case of substitutional randomness, there exist magnetic atoms in the nonmagnetic layers and nonmagnetic atoms in the magnetic layers near the interfaces. In other words, there are mixed layers of magnetic and nonmagnetic atoms at the interfaces. In order to deal with these mixed layers and the artificial periodicity of the multilayers, we adopt a cellular method where long unit cells are taken along the direction perpendicular to the layer planes. It is important to note that the cellular method[52] can treat the resistivities for currents parallel and perpendicular to layer planes consistently. We make use of the coherent potential approximation[53–55] (CPA) to formulate the expression of the resistivity caused by the interfacial randomness. The formalism will be explained in the next section. Numerical calculations, however, will be done in a weak scattering limit by using a single-band tight-binding model and the results of the computation and their interpretation will be given in Sec. III. We will show that $MR_\perp > MR_\parallel$ and the origin of this result will be attributed to the fact that the anisotropy of the resistivity, which is caused by the anisotropy of the effective mass of electron and the two-dimensional distribution of randomness at the interfaces, depends on the spin-dependent potential.

II. MODEL AND METHOD

In this section, we first summarize the single-cell CPA. Then, the expression for the resistivity is formulated in the same approximation, followed by explanations of the model to be used and the application of the derived expressions.

A. Formulation of resistivity in cell CPA

In deriving the cell CPA, we consider the disordered material which is divided into nonoverlapping equivalent cells. The Hamiltonian of this system consists of a purely site diagonal part $\hat{U}$ and a purely site off-diagonal part $\hat{W}$ as follows:

$$\hat{H} = \hat{W} + \hat{U}\,, \tag{1}$$

where $\hat{U}$ is, of course, cell diagonal and $\hat{W}$ is translationally invariant with respect to cells. In order to describe the cellular structure, we choose $|C,\mu\rangle$ $(=|C\rangle\otimes|\mu\rangle)$ for the basis vector where C and μ denote the indices of the cell and the site within the cell, respectively. Using this basis, $\hat{W}$ and $\hat{U}$ are rewritten as

$$\hat{W} = \sum_{C,C'} |C\rangle\, \mathbf{W}_{C,C'}\, \langle C'|\,, \tag{2}$$

$$\hat{U} = \sum_{C} |C\rangle\, \mathbf{U}_C\, \langle C|\,. \tag{3}$$

Since $\mathbf{W}_{C,C'}$ depends only $C - C'$ because of translational invariance, $\hat{W}$ becomes $\mathbf{k}$ diagonal by the following Fourier transformations:

$$|C\rangle = \frac{1}{\sqrt{N}} \sum_{\mathbf{k}} e^{-i\mathbf{k}\cdot\mathbf{R}_C} |\mathbf{k}\rangle\,, \tag{4a}$$

$$|\mathbf{k}\rangle = \frac{1}{\sqrt{N}} \sum_{C} e^{i\mathbf{k}\cdot\mathbf{R}_C} |C\rangle\,, \tag{4b}$$

where N, $\mathbf{R}_C$, and $\mathbf{k}$ are the number of cells in the system, the position vector of Cth cell, and the wave vector, respectively. In this transformation, $\hat{W}$ becomes

$$\hat{W} = \sum_{\mathbf{k}} |\mathbf{k}\rangle\, \mathbf{W}_{\mathbf{k}}\, \langle \mathbf{k}|\,, \tag{5}$$

$$\mathbf{W}_{\mathbf{k}} = \frac{1}{N} \sum_{C,C'} \mathbf{W}_{C,C'} e^{-i\mathbf{k}\cdot(\mathbf{R}_C - \mathbf{R}_{C'})}\,. \tag{6}$$

We assume site diagonal disorder due to the substitutional randomness of atoms. Then $\mathbf{U}_C$ depends on cells. The configurational average of any physical quantity over all random configurations in a cell is independent of the cell. Then we focus our attention on any single cell and replace the surrounding material by an effective medium $\hat{\Sigma}$, which possesses the translational invariance of the cell. The effective medium is cell diagonal and cell independent, that is,

$$\hat{\Sigma} = \sum_C |C\rangle \boldsymbol{\sigma} \langle C| . \tag{7}$$

The Green's function can be expanded in terms of $(\hat{U} - \hat{\Sigma})$,

$$\begin{aligned}\hat{G} &\equiv (z - \hat{H})^{-1} \\ &= \hat{\mathcal{G}} + \hat{\mathcal{G}}(\hat{U} - \hat{\Sigma})\hat{\mathcal{G}} + \hat{\mathcal{G}}(\hat{U} - \hat{\Sigma})\hat{\mathcal{G}}(\hat{U} - \hat{\Sigma})\hat{\mathcal{G}} + \cdots \\ &= \hat{\mathcal{G}} + \hat{\mathcal{G}}\hat{T}\hat{\mathcal{G}} ,\end{aligned} \tag{8}$$

where $\hat{\mathcal{G}}$ and $\hat{T}$ are the effective Green's function and the full T matrix, respectively, defined as

$$\hat{\mathcal{G}} = (z - \hat{W} - \hat{\Sigma})^{-1} , \tag{9}$$

$$\hat{T} = (\hat{U} - \hat{\Sigma})(1 + \hat{\mathcal{G}}\hat{T}) . \tag{10}$$

The full T matrix is rewritten by using the corresponding single-cell t matrix $\hat{t}_C$ as

$$\begin{aligned}\hat{T} = &\sum_C \hat{t}_C + \sum_{C \neq C'} \hat{t}_C \hat{\mathcal{G}} \hat{t}_{C'} \\ &+ \sum_{C \neq C', C' \neq C''} \hat{t}_C \hat{\mathcal{G}} \hat{t}_{C'} \hat{\mathcal{G}} \hat{t}_{C''} + \cdots .\end{aligned} \tag{11}$$

The single-cell t matrix is defined as

$$\hat{t}_C = |C\rangle \mathbf{t}_C \langle C| , \tag{12}$$

$$\mathbf{t}_C = (\mathbf{U}_C - \boldsymbol{\sigma})\,[1 - \boldsymbol{\mathcal{G}}_{CC}(\mathbf{U}_C - \boldsymbol{\sigma})]^{-1} . \tag{13}$$

The cell diagonal element of Green's function is

$$\begin{aligned}\boldsymbol{\mathcal{G}}_{CC} &= \langle C | \hat{\mathcal{G}} | C \rangle \\ &= \frac{1}{N} \sum_{\mathbf{k}} \boldsymbol{\mathcal{G}}_{\mathbf{k}} ,\end{aligned} \tag{14}$$

$$\boldsymbol{\mathcal{G}}_{\mathbf{k}} = (z\mathbb{1} - \mathbf{W}_{\mathbf{k}} - \boldsymbol{\sigma})^{-1} , \tag{15}$$

where the quantities $\mathbf{t}_C$, $\mathbf{U}_C$, $\boldsymbol{\sigma}$, $\boldsymbol{\mathcal{G}}_{CC}$, and $\boldsymbol{\mathcal{G}}_{\mathbf{k}}$ are $n \times n$ matrices if n atoms are in a cell and $\mathbb{1}$ denotes a n-dimensional unit matrix. It is assumed that the real Green's function averaged over all random configurations in a cell should equal to the corresponding Green's function of the effective medium itself. Hence,

$$\langle \hat{G} \rangle = \hat{\mathcal{G}} , \tag{16}$$

$$\langle \hat{T} \rangle = 0 , \tag{17}$$

where the brackets $\langle \cdots \rangle$ denote configurational average. This equation indicates that the effective medium produces no scattering of electrons on the average. Equation (17) is the exact self-consistent equation for determining the effective medium $\boldsymbol{\sigma}$ called the coherent potential. Instead of Eq. (17), however, a single-cell approximation is usually adopted. By decoupling the average in the right hand side of Eq. (11), we get

$$\begin{aligned}\langle \hat{T} \rangle \simeq \sum_{C \neq C', C' \neq C''} &\langle \hat{t}_C \rangle \Big(1 + \hat{\mathcal{G}} \langle \hat{t}_{C'} \rangle + \hat{\mathcal{G}} \langle \hat{t}_{C'} \rangle \hat{\mathcal{G}} \langle \hat{t}_{C''} \rangle \\ &+ \cdots \Big) .\end{aligned} \tag{18}$$

Then, the self-consistent equation in the single-cell approximation is $\langle \hat{t}_C \rangle = 0$, that is,

$$\langle (\mathbf{U}_C - \boldsymbol{\sigma})\,[\mathbb{1} - \boldsymbol{\mathcal{G}}_{CC}(\mathbf{U}_C - \boldsymbol{\sigma})]^{-1} \rangle = 0 , \tag{19}$$

which is an extension of the single-site CPA equation.

In deriving the expression for the electrical resistivity ρ, we start from the Kubo formula

$$\rho^{-1} = \frac{2\pi e^2}{\Omega} \operatorname{Tr} \langle \hat{v}\, \delta(E_F - \hat{H})\, \hat{v}\, \delta(E_F - \hat{H}) \rangle , \tag{20}$$

where Ω, $\hat{v}$, and E_F are the volume of the system, velocity operator, and the Fermi energy, respectively. In Eq. (20), the δ function is defined as

$$\delta(E_F - \hat{H}) = \frac{1}{2\pi i} \left[\hat{G}(z_-) - \hat{G}(z_+) \right] , \tag{21}$$

where $z_\pm = E_F \pm i\eta$ and η is an infinitesimal small positive number. To calculate the electrical resistivity, it is necessary to evaluate a configurational average of products of two Green's functions such as

$$\hat{K}(z_1, v, z_2) = \langle \hat{G}(z_1)\, \hat{v}\, \hat{G}(z_2) \rangle . \tag{22}$$

We first substitute Eq. (8) into Eq. (22); then

$$\hat{K} = \hat{\mathcal{K}} + \hat{\mathcal{G}}\hat{\Gamma}\hat{\mathcal{G}} , \tag{23}$$

$$\hat{\mathcal{K}} = \hat{\mathcal{G}}\hat{v}\hat{\mathcal{G}} , \tag{24}$$

$$\hat{\Gamma} = \langle \hat{T}\hat{\mathcal{G}}\hat{v}\hat{\mathcal{G}}\hat{T} \rangle , \tag{25}$$

where the second term of Eq. (23) is a vertex correction and $\hat{\Gamma}$ is called a vertex operator. In order to evaluate $\hat{\Gamma}$, we use Eq. (11) and apply a decoupling scheme which is consistent with the single-cell approximation in Eq. (18). As the result of the decoupling, the vertex correction becomes cell diagonal and cell independent:

$$\hat{\Gamma} = \sum_C |C\rangle \boldsymbol{\Gamma} \langle C| , \tag{26}$$

$$\boldsymbol{\Gamma} = \langle \mathbf{t}_C \mathbf{K}_{CC} \mathbf{t}_C \rangle - \langle \mathbf{t}_C \boldsymbol{\mathcal{G}}_{CC} \boldsymbol{\Gamma} \boldsymbol{\mathcal{G}}_{CC} \mathbf{t}_C \rangle , \tag{27}$$

$$\mathbf{K}_{CC} = \boldsymbol{\mathcal{K}}_{CC} + \sum_{C'} \boldsymbol{\mathcal{G}}_{CC'} \boldsymbol{\Gamma} \boldsymbol{\mathcal{G}}_{C'C} , \tag{28}$$

where $\boldsymbol{\mathcal{K}}_{CC} = \langle C | \hat{\mathcal{G}}\hat{v}\hat{\mathcal{G}} | C \rangle$. The vertex correction can be derived by solving Eqs. (27) and (28). In the single-cell CPA, the Kubo formula Eq. (20) is reduced to

$$\rho^{-1} = \frac{2\pi e^2}{\Omega} (I_0 + I_v) , \tag{29}$$

$$\begin{aligned}I_0 = &\frac{1}{4\pi^2} \sum_{\lambda_1, \lambda_2} \sum_C \operatorname{Tr} \left[\left(\hat{v}\, \hat{\mathcal{G}}(z_1)\, \hat{v}\, \hat{\mathcal{G}}(z_2) \right)_{CC} \right] \\ &\times (-1)^{(\lambda_1 + \lambda_2)/2} ,\end{aligned} \tag{30}$$

$$I_v = \frac{1}{4\pi^2} \sum_{\lambda_1,\lambda_2} \sum_{C} \mathrm{Tr}\left[\mathcal{K}_{CC}(z_1, v, z_2)\, \Gamma(z_2, v, z_1)\right] \times (-1)^{(\lambda_1+\lambda_2)/2}, \tag{31}$$

where $z_j = E_F + i\eta\lambda_j$, $\lambda_j = \pm 1$ $(j = 1, 2)$, and $\hat{I}_v$ is the vertex correction.

B. Model

We consider an A/B multilayer where the A and B layers consist of n_A and n_B atomic planes, respectively. In this section, we restrict ourselves to the case $n_A = 1$, $n_B = 2$ and formulate the expression for the resistivity. It is, however, quite easy to extend the expression derived in this section to other cases. We adopt the single-band tight-binding model to describe this multilayer. And we assume that the structure of this multilayer is a simple cubic lattice with lattice constant 1. Atomic layers are stacked along the (0, 0, 1) direction and the layer planes are assumed to be parallel to the x-y direction.

We now partition the multilayer into small equivalent cells. The periodicities along x and y directions are the same as those of the simple cubic structure. However, the periodicity of the unit cell along the z direction is n lattice spacings with $n = 2$ $(n_A + n_B)$, so that the unit cell has a (1, 1, n) structure. It is convenient to choose $n = 2$ $(n_A + n_B)$, instead of $(n_A + n_B)$, for the following motives. In case of magnetic multilayers A/B where A and B atoms are magnetic and nonmagnetic atoms, respectively, the adjacent magnetic A layers couple ferromagnetically in an external magnetic field but couple antiferromagnetically in the absence of the field. In order to treat the magnetic multilayer, it is necessary to choose $A|B|A'|B$ as the period. For ferromagnetic coupling, A and A' layers are equivalent. However, these layers are not equivalent for antiferromagnetic coupling because the magnetization direction of the A' layer is opposite to that of the A layer. As for the randomness at the interfaces, we only consider the substitutional randomness of A (A') and B atoms. Let ν and ν' denote the sites of A and A' atoms in the cell, respectively. We assume that A (A') atoms are replaced by B atoms with a concentration c at the $\mu = \nu$ (ν') site.

The Hamiltonian of this system consists of a purely off-diagonal part $\hat{W}$ and a purely diagonal part $\hat{U}$ as follows:

$$\hat{H} = \hat{W} + \hat{U} = -t \sum_{(i,j)} |\, i\,\rangle\langle\, j\,| + \sum_i u_i |\, i\,\rangle\langle\, i\,|, \tag{32}$$

where $|\, i\,\rangle$ is the Wannier state centered on the site i, the sum over (i, j) in the first term is restricted to a summation over all nearest neighbors, t is the hopping integral, and the atomic potential u_i is equal to u_A, $u_{A'}$, or u_B when the site i is occupied by an A, A', or B atom. By using the basis $|\, C, \mu\rangle$, which denotes the state at site $\mu(= 1 \sim n)$ in the Cth cell, $\hat{W}$ is rewritten as

$$\hat{W} = \sum_{C,C'}^{\parallel} |\, C\,\rangle\, \mathbf{W}_{\parallel}\, \langle\, C'\,| + \sum_{C}^{\perp} |\, C\,\rangle\, \mathbf{W}_{\perp}\, \langle\, C\,| + \sum_{C,C'}^{\perp'} |\, C\,\rangle\, \mathbf{W}'_{\perp}\, \langle\, C'\,| + \sum_{C,C'}^{\perp''} |\, C\,\rangle\, \mathbf{W}''_{\perp}\, \langle\, C'\,|, \tag{33}$$

where the first term in the right-hand side describes the hopping of electrons between cells in the x-y plane, the second term describes the hopping within a cell, and the third and fourth terms describe the hopping between cells along the z axis. The sums over C, C' in the first, third, and last term on the right-hand side of Eq. (33) are restricted to summations over all nearest neighbor cells under the condition $z_C = z_{C'}$, $z_C > z_{C'}$, and $z_C < z_{C'}$, respectively, where $z_C(z_{C'})$ denotes the z component of the position vector of $C(C')$th cell. The quantities $\mathbf{W}_{\parallel}$, $\mathbf{W}_{\perp}$, $\mathbf{W}'_{\perp}$, and $\mathbf{W}''_{\perp}$ are $n \times n$ matrices defined as

$$\mathbf{W}_{\parallel} \doteq -t\, \mathbb{1}, \tag{34}$$

$$\mathbf{W}_{\perp} \doteq \begin{pmatrix} 0 & -t & 0 & 0 & 0 & 0 \\ -t & 0 & -t & 0 & 0 & 0 \\ 0 & -t & 0 & -t & 0 & 0 \\ 0 & 0 & -t & 0 & -t & 0 \\ 0 & 0 & 0 & -t & 0 & -t \\ 0 & 0 & 0 & 0 & -t & 0 \end{pmatrix}, \tag{35}$$

$$\mathbf{W}'_{\perp} \doteq \begin{cases} -t & : (1, n) \text{ element}, \\ 0 & : \text{others}, \end{cases} \tag{36}$$

$$\mathbf{W}''_{\perp} \doteq \begin{cases} -t & : (n, 1) \text{ element}, \\ 0 & : \text{others}, \end{cases} \tag{37}$$

where the symbol $\doteq$ stands for "is represented by the basis vector $|\, \mu\,\rangle$." By using the Fourier transformation Eq. (4), $\hat{W}$ is rewritten as

$$\hat{W} = \sum_{\mathbf{k}} |\, \mathbf{k}\,\rangle\, \mathbf{W}_{\mathbf{k}}\, \langle\, \mathbf{k}\,|, \tag{38}$$

$$\mathbf{W}_{\mathbf{k}} \doteq \begin{pmatrix} \epsilon_{\mathbf{k}_{\parallel}} & -t & 0 & 0 & 0 & -te^{-ik_z n} \\ -t & \epsilon_{\mathbf{k}_{\parallel}} & -t & 0 & 0 & 0 \\ 0 & -t & \epsilon_{\mathbf{k}_{\parallel}} & -t & 0 & 0 \\ 0 & 0 & -t & \epsilon_{\mathbf{k}_{\parallel}} & -t & 0 \\ 0 & 0 & 0 & -t & \epsilon_{\mathbf{k}_{\parallel}} & -t \\ -te^{ik_z n} & 0 & 0 & 0 & -t & \epsilon_{\mathbf{k}_{\parallel}} \end{pmatrix}, \tag{39}$$

where $-\pi \le k_x, k_y \le \pi$, $-\pi/n \le k_z \le \pi/n$, and $\epsilon_{\mathbf{k}_{\parallel}} = -2t(\cos k_x + \cos k_y)$.

In a similar way, $\hat{U}$ is rewritten as

$$\hat{U} = \sum_{C} |\, C\,\rangle\, \mathbf{U}_C\, \langle\, C\,|, \tag{40}$$

$$\mathbf{U}_C \doteq \begin{pmatrix} u_B & 0 & 0 & 0 & 0 & 0 \\ 0 & u_{C,\nu} & 0 & 0 & 0 & 0 \\ 0 & 0 & u_B & 0 & 0 & 0 \\ 0 & 0 & 0 & u_B & 0 & 0 \\ 0 & 0 & 0 & 0 & u_{C,\nu'} & 0 \\ 0 & 0 & 0 & 0 & 0 & u_B \end{pmatrix}, \tag{41}$$

where $u_{C,\nu(\nu')}$ is $u_{A(A')}$, if the site $\nu(\nu')$ in the Cth cell is occupied by an $A(A')$ atom, and u_B if it is occupied

by a B atom.

Since randomness exists only on the ν and ν' sites, the coherent potential, which is derived by solving Eqs. (14) and (19) self-consistently, is written as

$$\boldsymbol{\sigma} \doteq \begin{pmatrix} u_B & 0 & 0 & 0 & 0 & 0 \\ 0 & \sigma^{\nu\nu} & 0 & 0 & \sigma^{\nu\nu'} & 0 \\ 0 & 0 & u_B & 0 & 0 & 0 \\ 0 & 0 & 0 & u_B & 0 & 0 \\ 0 & \sigma^{\nu'\nu} & 0 & 0 & \sigma^{\nu'\nu'} & 0 \\ 0 & 0 & 0 & 0 & 0 & u_B \end{pmatrix} . \tag{42}$$

The numerical calculation will be performed in the weak scattering limit. In this limit, the coherent potential is reduced to

$$\boldsymbol{\sigma} = \langle \mathbf{U}_C \rangle + \langle (\mathbf{U}_C - \langle \mathbf{U}_C \rangle) \boldsymbol{\mathcal{G}}_{CC} (\mathbf{U}_C - \langle \mathbf{U}_C \rangle) \rangle . \tag{43}$$

It should be noted that $\boldsymbol{\sigma}$ involved in $\boldsymbol{\mathcal{G}}_{CC}$ in Eq. (43) is replaced by $\langle \mathbf{U}_C \rangle$ and that the imaginary part of the last term of Eq. (43) describes the effect of the scattering due to randomness. The matrix elements of the coherent potential are

$$\sigma^{\nu\nu} = cu_A + (1-c)u_B + c(1-c)(u_A - u_B)^2 \mathcal{G}^{\nu\nu}_{CC} , \tag{44a}$$

$$\sigma^{\nu'\nu'} = cu_{A'} + (1-c)u_B + c(1-c)(u_{A'} - u_B)^2 \mathcal{G}^{\nu'\nu'}_{CC} , \tag{44b}$$

$$\sigma^{\nu\nu'} = \sigma^{\nu'\nu} = 0 , \tag{44c}$$

where $\boldsymbol{\sigma}$'s involved in $\mathcal{G}^{\nu\nu}_{CC} (= \langle \nu | \boldsymbol{\mathcal{G}}_{CC} | \nu \rangle)$ and $\mathcal{G}^{\nu'\nu'}_{CC} (= \langle \nu' | \boldsymbol{\mathcal{G}}_{CC} | \nu' \rangle)$ are replaced by $\langle \mathbf{U}_C \rangle$ as mentioned above.

Next, we derive the velocity operator, which is defined as

$$\hat{v}_\alpha = \frac{1}{i\hbar} [\hat{R}_\alpha, \hat{H}] \quad (\alpha = x, y, z) , \tag{45}$$

where $\hat{R}_\alpha$ is the site-position operator. From Eqs. (4) and (33), the velocity operator $\hat{v}_\alpha$ becomes $\mathbf{k}$ diagonal:

$$\hat{v}_\alpha = \sum_{\mathbf{k}} | \mathbf{k} \rangle \mathbf{v}_{\mathbf{k},\alpha} \langle \mathbf{k} | , \tag{46}$$

$$\mathbf{v}_{\mathbf{k}x(y)} \doteq \frac{2t}{\hbar} \sin k_{x(y)} \mathbb{1} , \tag{47}$$

$$\mathbf{v}_{\mathbf{k}z} \doteq \frac{t}{\hbar} \begin{pmatrix} 0 & -i & 0 & 0 & 0 & ie^{-ik_z n} \\ i & 0 & -i & 0 & 0 & 0 \\ 0 & i & 0 & -i & 0 & 0 \\ 0 & 0 & i & 0 & -i & 0 \\ 0 & 0 & 0 & i & 0 & -i \\ -ie^{ik_z n} & 0 & 0 & 0 & i & 0 \end{pmatrix} . \tag{48}$$

Using the $| \mathbf{k} \rangle$ representation, $\boldsymbol{\mathcal{K}}_{CC}$ in the vertex correction term Eq. (31) becomes

$$\boldsymbol{\mathcal{K}}_{CC}(z_1, v_\alpha, z_2) = \frac{1}{N} \sum_{\mathbf{k}} \boldsymbol{\mathcal{G}}_{\mathbf{k}}(z_1) \mathbf{v}_{\mathbf{k},\alpha} \boldsymbol{\mathcal{G}}_{\mathbf{k}}(z_2) . \tag{49}$$

Since $\boldsymbol{\mathcal{G}}_{\mathbf{k}}$ and $\mathbf{v}_{\mathbf{k},x(y)}$ are even and odd functions of $k_{x(y)}$, respectively, $\boldsymbol{\mathcal{K}}_{CC}$ vanishes for x and y directions; i.e., the vertex correction for the currents along x and y directions vanishes. However, since $\mathbf{v}_{\mathbf{k},z}$ is not an odd function of k_z, the vertex correction for the current along z direction does not necessarily vanish. We found, however, that this vertex correction is negligibly small in our numerical calculation.

III. CALCULATED RESULTS

At the beginning of this section, we show the validity of our method and calculation. We consider a nonmagnetic multilayer A/B, with a configuration of atoms within the unit cell as shown in the inset of Fig. 1. At the shaded sites, A and B atoms are randomly distributed, each with concentration 0.5. The potentials of the A and B atoms are taken to be $0.3t$ and $-0.3t$, respectively. Calculated results for ρ^{-1}, i.e., the conductivity, are shown in Fig. 1 as functions of E_F, where $\parallel$ and $\perp$ denote directions parallel and perpendicular to the layer planes, respectively. The dependence of ρ^{-1} on E_F is quite similar to that calculated for a random alloy.[55] The dips in $\rho_\parallel^{-1}$ and $\rho_\perp^{-1}$ are related to the Van Hove singularities of the density of states for the simple cubic structure. The similarity between our results and those calculated for a random alloy is considered to justify our method and calculation.

It is also noteworthy that the resistivity without the vertex correction term does not change in the weak scattering limit even if we use the unit cell whose structure is $(2,1,n)$, $(1,1,2n)$, etc., instead of $(1,1,n)$, and that the vertex correction is negligibly small in our numerical calculation.

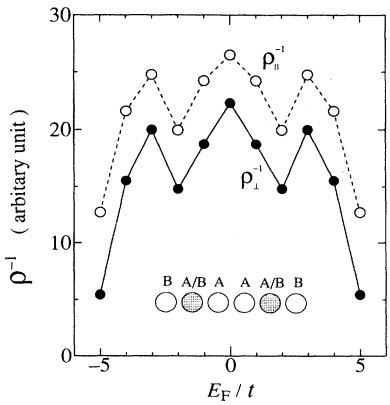

FIG. 1. Calculated results for the inverse of resistivity in a nonmagnetic multilayer for parallel (○) and perpendicular (●) currents as functions of E_F. Solid and dashed curves are guides to the eye. The inset shows the configuration of atoms within the unit cell.

A. $MR_{\|}$ and $MR_{\perp}$

We consider a magnetic multilayer A/B. The configuration of atoms within the unit cell is shown in Fig. 2, where A and A' atoms are magnetic atoms. Then, the potentials of the A and A' atoms, $u_{A,\sigma}$ and $u_{A',\sigma}$, depend on the spin $\sigma(=\uparrow,\downarrow)$. For ferromagnetic (F) alignment of adjacent magnetic layers, A and A' atoms are equivalent and $u_{A,\sigma} = u_{A',\sigma}$. However, for antiferromagnetic (AF) alignment, their magnetization directions are opposite to each other, and they are no longer equivalent, but instead $u_{A,\sigma} = u_{A',-\sigma}$. A schematic figure of the potential of each atom within the unit cell is shown in Fig. 2. We assume that the spin-dependent potentials of the A and A' atoms are given to be $\pm 0.5t$ and treat the spin-independent potential of the B atom, u_B, as a variable parameter. We further assume that A and A' atoms are replaced by B atoms with a concentration $c = 0.5$.

First, we show the calculated results for the spin-dependent resistivities in F and AF alignments for parallel and perpendicular currents in Fig. 3 as functions of u_B. For AF alignment, since resistivities for $\uparrow$ and $\downarrow$ spin electrons are the same, only resistivities for $\downarrow$ spin electron, $\rho_{\downarrow AF}$, are plotted. As the potential difference for $\downarrow$ spin states, $|u_{A\downarrow} - u_B|$, decreases with increasing u_B, the resistivity for $\downarrow$ spin electrons in ferromagnetic alignment, $\rho_{\downarrow F}$, becomes small. On the contrary, the potential difference for $\uparrow$ spin state, $|u_{A\uparrow} - u_B|$, increases with u_B, so that the resistivity for $\uparrow$ spin electrons, $\rho_{\uparrow F}$, becomes large. Thereby $\rho_{\downarrow AF}$ is always larger than $\rho_{\downarrow F}$ and smaller than $\rho_{\uparrow F}$. The figure also shows that the resistivities for perpendicular current are always larger than those for parallel currents.

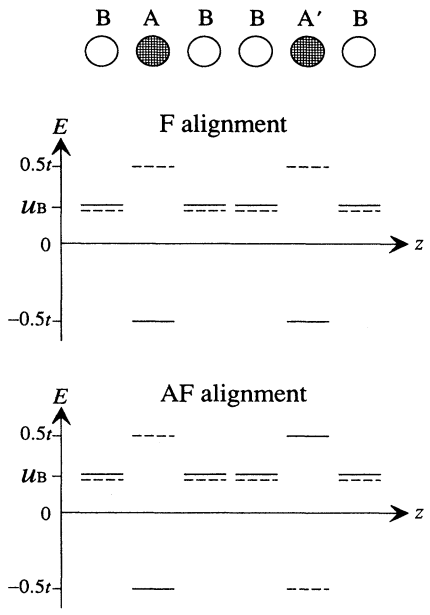

FIG. 2. Configuration of atoms within the unit cell and the level scheme of potentials of each atom which is used in the calculation of MR ratio; the results are shown in Fig. 4. Solid and dashed lines are potentials of each atom for $\uparrow$ and $\downarrow$ spin states, respectively.

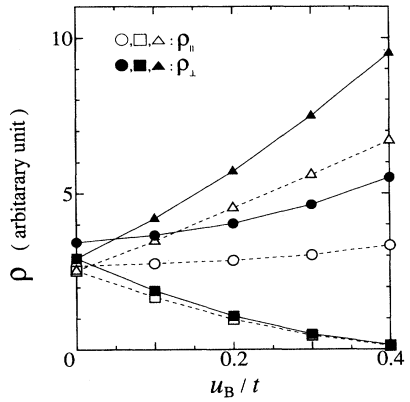

FIG. 3. Calculated results for the resistivities in a magnetic multilayer for parallel (open symbols) and perpendicular (solid symbols) currents as functions of u_B. Triangles, squares, and circles are the results for $\rho_{\uparrow F}$, $\rho_{\downarrow F}$, and$\rho_{\downarrow AF}$, respectively. Solid and dashed curves are guides to the eye.

Next, we study the MR ratio which is defined as $(\rho_{AF} - \rho_F)/\rho_{AF}$ where ρ_F and ρ_{AF} are calculated by using the two currents model, that is,

$$\rho_{F(AF)} = \left(\rho^{-1}_{\uparrow F(AF)} + \rho^{-1}_{\downarrow F(AF)}\right)^{-1} . \tag{50}$$

The calculated results of MR ratios, $MR_{\|}$ and $MR_{\perp}$, are shown in Fig. 4 as functions of E_F for several values of u_B. The following characteristics can be noticed from the figure. When $u_B = 0.4t$, the MR ratios for both parallel and perpendicular currents are nearly the maximum value, i.e., $MR_{\|} \sim MR_{\perp} \sim 1.0$. The reason is that $\rho_{F\|} \sim \rho_{F\|\downarrow} \sim \rho_{F\perp} \sim \rho_{F\perp\downarrow} \sim 0$ because of a good level matching for $\downarrow$ spin states, that is, $u_{A\downarrow} \sim u_B$. A notable difference between $MR_{\|}$ and $MR_{\perp}$ can be observed

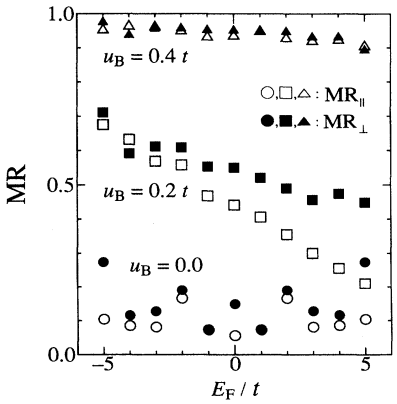

FIG. 4. Calculated results for the MR ratios for parallel (open symbols) and perpendicular (solid symbols) currents as functions of E_F. Triangles, squares, and circles are the results for $u_B = 0.4t$, $0.2t$, and 0, respectively.

when $u_B = 0.2t$. Even when $u_B = 0.0$—that is, the potential differences $|u_{A\sigma} - u_B|$ for $\uparrow$ and $\downarrow$ spin states are the same—the MR ratio is nonzero and $\mathrm{MR}_\perp \geq \mathrm{MR}_\parallel$. The dependence of the MR ratio on E_F is asymmetric with respect to $E_F = 0$ except for the results with $u_B = 0.0$. This is because the potential is asymmetric with respect to the origin of the energy. We may conclude from the calculated results shown in Fig. 4 that a tendency towards $\mathrm{MR}_\perp > \mathrm{MR}_\parallel$ exists. In the next subsection, we will give an interpretation for the numerical results and clarify the physical origins of the results that $\mathrm{MR}_\perp > \mathrm{MR}_\parallel$.

At the end of this subsection, we would like to note that the present definition of the MR ratio is given by $(\rho_{\mathrm{AF}} - \rho_{\mathrm{F}})/\rho_{\mathrm{AF}}$ and thereby the maximum value of the MR ratio is 1.0. Therefore, the small difference between $\mathrm{MR}_\perp$ and $\mathrm{MR}_\parallel$ for $u_B = 0.4t$ does not necessarily mean a small difference between $\rho_{\mathrm{F}\parallel}/\rho_{\mathrm{AF}\parallel}$ and $\rho_{\mathrm{F}\perp}/\rho_{\mathrm{AF}\perp}$. The experimental values of the MR ratio in the present definition are about 0.2 and 0.5 for the parallel and perpendicular currents, respectively, typically for Co/Cu and Fe/Cr multilayers.[12,15]

B. Interpretation of the numerical results

In this subsection, we will give the interpretation of the general trend that $\mathrm{MR}_\perp > \mathrm{MR}_\parallel$ obtained in the previous subsection and clarify the origins of the trend. There are several factors which affect the MR; that is, the resistivity depends on the potentials which are spin dependent, on the direction of the currents, and on the change in the periodicity. To separate these factors from each other, we adopt the following procedures. First, we consider a nonmagnetic multilayer A/B and study how the resistivity is affected by the direction of the currents and by the change in the periodicity.

Figure 5 shows the calculated results of the dependence of $\rho_\parallel$ and $\rho_\perp$ on the random potential. The configuration of atoms within the unit cell is shown in the inset of Fig. 5. The value of u_B is 0 and u_A is taken as a variable parameter. We assume that A atoms are replaced by B atoms with a concentration 0.5. The value E_F is taken to be 0.0. These results show that $\rho_\perp$ is always larger than $\rho_\parallel$. Both $\rho_\parallel$ and $\rho_\perp$ are proportional roughly to u_A^2 as expected. The deviation may be due to the interference effect.

In Born approximation, the resistivity for the direction $\alpha(=\parallel, \perp)$ is given by

$$\rho_\alpha^{-1} = e^2 \tau \langle (V_\alpha)^2 \rangle D(E_F)\,, \tag{51}$$

where τ, $D(E)$, and $\langle (V_\alpha)^2 \rangle$ are the lifetime, the density of states, and the square of the Fermi velocity, respectively. The square of the Fermi velocity is defined by

$$\langle (V_\alpha)^2 \rangle = \frac{\sum_{\mathbf{k}} \{v_\alpha(\mathbf{k})\}^2 \delta(E_F - E(\mathbf{k}))}{\sum_{\mathbf{k}} \delta(E_F - E(\mathbf{k}))}\,, \tag{52}$$

$$v_\alpha(\mathbf{k}) = \frac{1}{\hbar} \frac{\partial E(\mathbf{k})}{\partial k_\alpha}\,, \tag{53}$$

where $E(\mathbf{k})$ is the energy eigenvalue of the Bloch state with wave vector $\mathbf{k}$, and is calculated in virtual crystal approximation where $\mathbf{U}_C$ in the Hamiltonian is replaced by its averaged value $\langle \mathbf{U}_C \rangle$; then $\boldsymbol{\sigma} = \langle \mathbf{U}_C \rangle$. In this case, the difference between $\rho_\parallel$ and $\rho_\perp$ is caused only by the anisotropy of the Fermi velocity, i.e., the anisotropy of the effective mass.[56] The ratio $\langle (V_\parallel)^2 \rangle / \langle (V_\perp)^2 \rangle$ as well as $\rho_\perp/\rho_\parallel$ are shown in Fig. 6 as functions of u_A, where the resistivities $\rho_\parallel$ and $\rho_\perp$ are already shown in Fig. 5. The value $\langle (V_\parallel)^2 \rangle / \langle (V_\perp)^2 \rangle$ represents the anisotropy of the effective mass of electrons due to the miniband structures of the electronic states. The miniband structures originate from the layered structure of the multilayer which is reflected in the artificial periodicity of $\langle \mathbf{U}_C \rangle$. The anisotropy of the effective mass becomes large with increasing value of u_A, as well as the anisotropy of resis-

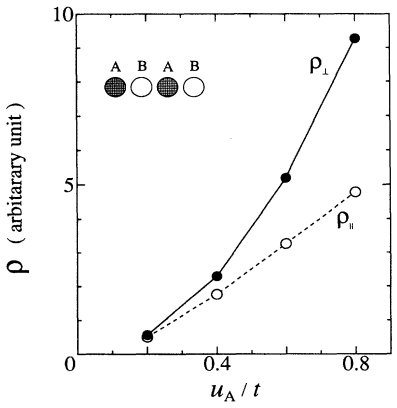

FIG. 5. Calculated results for the resistivities in a nonmagnetic multilayer for parallel (○) and perpendicular (●) currents as functions of u_A. Solid and dashed lines are guides to the eye. The inset shows the configuration of atoms within the unit cell used in the calculation.

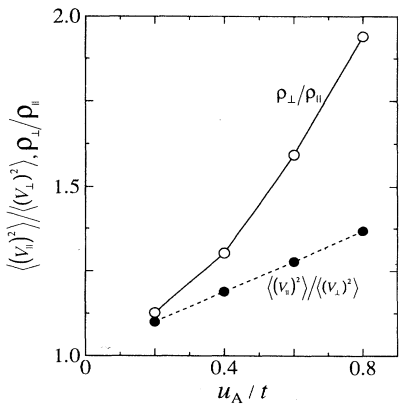

FIG. 6. Calculated results for the ratios $\langle (V_\parallel)^2 \rangle / \langle (V_\perp)^2 \rangle$ (○) and $\rho_\perp/\rho_\parallel$ (●) in a nonmagnetic multilayer. The resistivity $\rho_\parallel$ and $\rho_\perp$ are already shown in Fig. 5. Solid and dashed curves are guides to the eye.

tivity. However, it is clear that the anisotropy of the effective mass is not enough to explain the anisotropy of the resistivity because $\rho_\perp/\rho_\parallel$ increases more rapidly than $\langle(V_\parallel)^2\rangle/\langle(V_\perp)^2\rangle$ as u_A increases.

The difference between $\rho_\perp/\rho_\parallel$ and $\langle(V_\parallel)^2\rangle/\langle(V_\perp)^2\rangle$ can be caused by the two-dimensional distribution of the randomness at the interfaces. The coherent potential has imaginary parts, which describe the effect of the scattering due to the randomness at the interfaces as shown in Eq. (44). When there are equivalent imaginary parts at every site; that is, the second term of Eq. (43) is replaced by $i\Delta\mathbb{1}$ (Δ is a positive number small compared with the hopping integral t), then the ratio $\rho_\perp/\rho_\parallel$ coincides with $\langle(V_\parallel)^2\rangle/\langle(V_\perp)^2\rangle$ which is already shown in Fig. 6. It has been checked that the resistivity hardly changes even if the real part of the last term of Eq. (43) is fixed to be 0. Therefore, the anisotropy of the resistivity must be enhanced by the two-dimensional distribution of randomness at the interfaces.

The thickness dependence of $\rho_\parallel$ and $\rho_\perp$ is shown in Fig. 7. Here, u_A, u_B, n_A, and E_F are taken to be $0.8t$, 0.0, 1, and $0.2t$, respectively, and the concentration of the random sites is the same as that used previously. As can be seen from Fig. 7, the inverse of resistivity is almost proportional to n_B. The result indicates that Ohm's law holds well.

Next, we study the dependence of $\rho_\perp/\rho_\parallel$ on the periodicity. The configuration of atoms within the unit cell and the concentration of the random sites are the same as those in Fig. 2. The value u_B is taken to be 0.0, and $|u_A|(=|u_{A'}|)$ is taken as a variable parameter. We call the configuration where $u_A = u_{A'}$ the symmetric (s) case, and call the configuration where $u_A = -u_{A'}$ the antisymmetric (a) case. The periodicity of the antisymmetric case is twice that of the symmetric case. The calculated results of $(\rho_\perp/\rho_\parallel)_{s(a)}$ for the symmetric (antisymmetric) case are shown in Fig. 8 as functions of u_A. The values of E_F are taken to be 0.0 and $1.0t$. We find that $(\rho_\perp/\rho_\parallel)_a > (\rho_\perp/\rho_\parallel)_s$ for $E_F = 0.0$, but

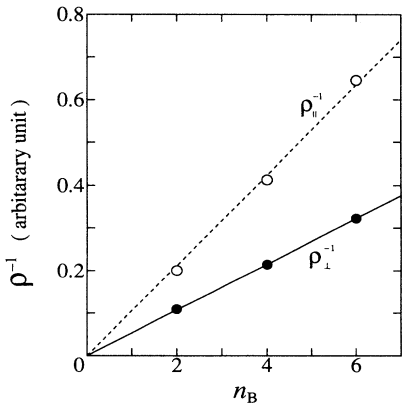

FIG. 7. Calculated results for the inverse of resistivities in a nonmagnetic multilayer for parallel (○) and perpendicular (●) currents as functions of n_B. Solid and dashed lines are guides to the eye.

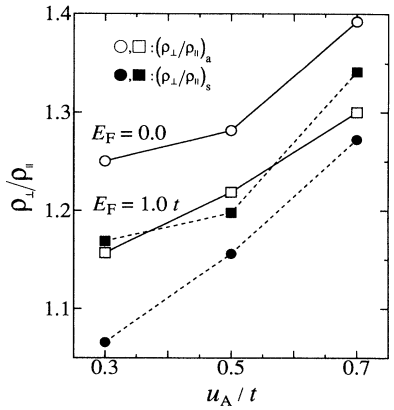

FIG. 8. Calculated results for the ratios $\rho_\parallel/\rho_\perp$ in a nonmagnetic multilayer for the symmetric (open symbols) and antisymmetric (solid symbols) cases mentioned in the text. Circles and squares are the results for $E_F = 0$ and $1.0t$, respectively. Solid and dashed curves are guides to the eye.

$(\rho_\perp/\rho_\parallel)_a \sim (\rho_\perp/\rho_\parallel)_s$ for $E_F = 1.0t$. The result that $(\rho_\perp/\rho_\parallel)_a \gtrsim (\rho_\perp/\rho_\parallel)_s$ may be attributed to the change of the effective mass especially for the perpendicular direction. By doubling the period of the unit cell along perpendicular direction, the size of the Brillouin zone is halved and band gaps appear at zone boundaries in k_z direction, so that the effective mass for perpendicular direction becomes large.

Thus, we have found that two factors, the anisotropy of the effective mass due to the miniband structure and the two-dimensional distribution of randomness at the interfaces, play important roles on the resistivities $\rho_\parallel$ and $\rho_\perp$. We would like to stress again that these two factors originate from the layered structure of the multilayer and that the effects of these two factors on the anisotropy of the resistivity become strong as the potential difference between A and B atoms increases.

Now, we interpret the calculated results shown in Fig. 4 including the spin-dependent resistivity. A simple interpretation, however, is possible only for two cases: the results for $u_B = 0.4t$ and 0.0. When $u_B = 0.4t$, because of the good level matching for $\downarrow$ spin state, we obtain $\rho_{F\parallel} \sim \rho_{\downarrow F\parallel}$ and $\rho_{F\perp} \sim \rho_{\downarrow F\perp}$ for F alignment. For AF alignment, we generally obtain that $\rho_{\uparrow AF} = \rho_{\downarrow AF}$ for both parallel and perpendicular currents, so that $\rho_{AF} = \rho_{\downarrow AF}/2$. For AF alignment, we can approximately neglect the scattering at A site for $\downarrow$ spin electron and it is enough to consider only the scattering at A' site, because of $|u_{A'\downarrow} - u_B| \gg |u_{A\downarrow} - u_B|$. From the result shown in Fig. 7 that $\rho_\perp/\rho_\parallel$ is independent of n_B, we can approximate $\rho_{\perp AF}/\rho_{\parallel AF} \sim \rho_{\uparrow\perp F}/\rho_{\uparrow\parallel F}$. Therefore, we get

$$\frac{1-\mathrm{MR}_\parallel}{1-\mathrm{MR}_\perp} = \frac{\rho_{\parallel F}/\rho_{\parallel AF}}{\rho_{\perp F}/\rho_{\perp AF}} = \frac{\rho_{\perp AF}/\rho_{\parallel AF}}{\rho_{\perp F}/\rho_{\parallel AF}} \sim \frac{\rho_{\uparrow\perp F}/\rho_{\uparrow\parallel F}}{\rho_{\downarrow\perp F}/\rho_{\downarrow\parallel F}} > 1.0\,, \tag{54}$$

that is, $\mathrm{MR}_\perp > \mathrm{MR}_\parallel$. To obtain the last inequality in

this equation, we used the results shown in Fig. 5 and the fact that the potential difference $|u_{A\uparrow} - u_B|$ is larger than $|u_{A\downarrow} - u_B|$. Here, the dependence of $\rho_\perp/\rho_\parallel$ on the potential difference plays an important role.

The other limiting case is that for $u_B = 0.0$. In this case, the MR ratios are not equal to 0 although the potential differences $|u_{A\sigma} - u_B|$ for $\uparrow$ and $\downarrow$ spin states are the same. The reason why the MR ratios are not equal to 0 and $\mathrm{MR}_\perp \geq \mathrm{MR}_\perp$ is attributed to the change of the effective mass due to the change in the periodicity.

It has been already pointed out that the anisotropy of the resistivity is caused by the anisotropy of the effective mass and the two-dimensional distribution of randomness and that the ratio $\rho_\perp/\rho_\parallel$ becomes larger as the potential difference between A and B atoms increases. When there is a good level matching in, say, the $\downarrow$ spin state as in the results in Fig. 4 with $u_B = 0.4t$, $(\rho_\perp/\rho_\parallel)_{\mathrm{F}}$ is much smaller than $(\rho_\perp/\rho_\parallel)_{\mathrm{AF}}$ because the potential difference between A and B atoms for the $\downarrow$ spin state in F alignment is much smaller than that for the $\uparrow$ and $\downarrow$ spin states in AF alignment. Therefore, we obtain $\rho_{\parallel\mathrm{F}} \sim \rho_{\perp\mathrm{F}}$ and $\rho_{\parallel\mathrm{AF}} < \rho_{\perp\mathrm{AF}}$, which results in $\mathrm{MR}_\parallel < \mathrm{MR}_\perp$. Because the large MR is caused by the good level matching in either $\uparrow$ or $\downarrow$ spin state, the asymmetry of the spin-dependent potential is crucial for both the MR and the difference between $\mathrm{MR}_\parallel$ and $\mathrm{MR}_\perp$. When there is no good level matching, the effect of the change in the periodicity becomes important as in the results in Fig. 4 with $u_B = 0.0$.

C. Dependence of MR on the randomness

In this subsection, we show the dependence of $\mathrm{MR}_\parallel$ and $\mathrm{MR}_\perp$ on the randomness at the interfaces, i.e., the concentration c . The configuration of atoms within the unit cell is the same as that used previously (see Fig. 2). The concentration c, with which A and A' atoms are replaced by B atoms, is taken as a variable parameter. Here, $u_{A,\sigma}$, u_B, and E_F are taken to be $\pm 0.5t$, $0.2t$, and $2.0t$, respectively. Figure 9 shows the calculated results for the concentration dependence of the MR ratio.

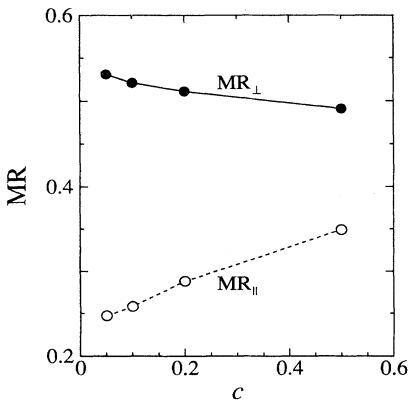

FIG. 9. Calculated results for the MR ratios for parallel (○) and perpendicular (●) directions as functions of c. Solid and dashed curves are guides to the eye.

These results show that $\mathrm{MR}_\parallel$ increases while $\mathrm{MR}_\perp$ decreases with increasing concentration c, which is qualitatively consistent with results derived by the numerical simulation.[50] The difference between $\mathrm{MR}_\parallel$ and $\mathrm{MR}_\perp$ may vanish in the limit of $c \to 1$, because almost all atoms included are B atoms and then both the anisotropy of the structure and the anisotropy of the randomness become weak. On the contrary, the difference between $\mathrm{MR}_\parallel$ and $\mathrm{MR}_\perp$ becomes large with decreasing c. In the dilute limit ($c \to 0$) in Fig. 9, both $\mathrm{MR}_\parallel$ and $\mathrm{MR}_\perp$ remain finite and $\mathrm{MR}_\perp > \mathrm{MR}_\parallel$. This is due to the effect of the effective mass on the resistivity. Thus, with decreasing the randomness, the anisotropy of the electron mass becomes dominant for the difference between $\mathrm{MR}_\parallel$ and $\mathrm{MR}_\perp$. The effect of the randomness seems to be more important for $\mathrm{MR}_\parallel$ than for $\mathrm{MR}_\perp$.

IV. DISCUSSION

In our numerical calculation, the vertex correction has been negligibly small. One reason is the treatment in the weak scattering limit. The other reason is that we have used small unit cells. The former is, however, less important because the weak scattering limit is a good approximation when the random potential is small enough as compared to the bandwidth and our calculations have been done in this range. In cell CPA, the intracell scattering is treated exactly, but the intercell scattering is treated approximately. It has been reported by Bauer *et al.*[46–48] that the vertex correction to the conductivity corresponds to a diffusive scattering of electrons at the interfaces where the electron momentum along layer planes is not conserved. In the cellular method, because the size of the unit cells is small, the momentum change is restricted and the vertex correction is reduced. The number of atoms in the unit cell used in the present calculations has been limited to no more than 6. The limitation is mainly due to the computational time for the three-dimensional integration over k_x, k_y, and k_z which is necessary to calculate $\rho_\parallel$. The integration is, however, reduced to the two-dimensional integration for $\rho_\perp$ by using the complete elliptic integral.[57] Although the resistivity itself can be evaluated more correctly by making the unit cell larger, the MR ratio may not be affected so much because it is a ratio of resistivities in AF and F alignments. The origin of the difference between $\mathrm{MR}_\perp$ and $\mathrm{MR}_\parallel$ may also hold to be correct.

We have shown that $\mathrm{MR}_\perp$ tends to be larger than $\mathrm{MR}_\parallel$, which is consistent with experimental results. Quantitatively, however, both $\mathrm{MR}_\parallel$ and $\mathrm{MR}_\perp$ are larger than the experimental ones. In Fig. 4, we get $\mathrm{MR}_\parallel \lesssim \mathrm{MR}_\perp \sim 1$ for the case $u_B = 0.4t$, which corresponds to a Fe/Cr multilayer in the sense that the potential difference between magnetic and nonmagnetic atoms is small for the $\downarrow$ spin state.[23] In a Fe/Cr multilayer, the observed MR ratios are about 0.2 and 0.5 for parallel and perpendicular directions, respectively.[15] The reason why the magnitude of the calculated MR ratios is larger than those of experiments is that only spin-dependent scattering at the

interfaces has been taken into account to calculate the resistivity. If we take into account the nonmagnetic scattering, the MR ratios become smaller and the difference between $MR_{\parallel}$ and $MR_{\perp}$ becomes more obvious.

Our result that $MR_{\perp} > MR_{\parallel}$ is consistent with results derived by Asano *et al.*[50] They attributed the origin of the difference between $MR_{\parallel}$ and $MR_{\perp}$ mainly to the miniband structure, which corresponds to the anisotropy of the effective mass in our expression. Because their treatment of the scattering is exact, their results must include the effects of various factors of layered structure. Further analysis, however, has not been made. In this paper, it has been pointed out that not only the anisotropy of the effective mass but also the two-dimensional distribution of randomness are important for the difference between $MR_{\parallel}$ and $MR_{\perp}$. It has been also found that the effects of the anisotropy of the effective mass and the two-dimensional distribution of randomness on the anisotropy of the resistivity become strong when the potential difference between magnetic and nonmagnetic atoms becomes large.

As for the dependence of MR on the randomness at the interfaces, we have shown that the difference between $MR_{\parallel}$ and $MR_{\perp}$ increases with decreasing the randomness. The results are also consistent with those by Asano *et al.*[50] We must be careful, however, to interpret their results because of the existence of the contact resistance. The contact resistance may be interpreted as the spin-independent resistivity, which naturally exists in real samples. However, when we discuss the dependence of MR on the magnitude of the randomness, the contact resistivity must be sufficiently smaller than the resistivity due to the randomness under consideration. Their results with strong randomness are sufficiently meaningful and are consistent with our present results.

V. SUMMARY

We have presented the cell CPA method to study the origin of the difference between $MR_{\parallel}$ and $MR_{\perp}$ in magnetic multilayers. In this method, randomness at the interfaces and layered structure can be treated simultaneously. The spin-dependent resistivity has been calculated by using the Kubo formalism in the weak scattering limit. It has been shown that $MR_{\perp}$ tends to be larger than $MR_{\parallel}$. Two factors have been pointed out to cause the difference between $MR_{\parallel}$ and $MR_{\perp}$. One is the anisotropy of the effective mass due to the miniband structure in the electronic states; the other is the two-dimensional distribution of randomness at the interfaces. These two factors originate from the layered structure of the multilayer. As the difference of the spin-dependent potentials between magnetic and nonmagnetic atoms increases, the effects of these two factors on the anisotropy of the resistivity become strong. Since the anisotropy of resistivity in F alignment is smaller than that in AF alignment because of a good level matching for $\uparrow$ or $\downarrow$ spin states, $MR_{\perp}$ becomes larger than $MR_{\parallel}$.

It has been also shown that $MR_{\perp}$ tends to increase with decreasing interfacial roughness, but $MR_{\parallel}$ tends to decrease. The results indicate that interfacial roughness is favorable for $MR_{\parallel}$ but not for $MR_{\perp}$. Experiments which verify the dependence of the difference between $MR_{\parallel}$ and $MR_{\perp}$ on the interfacial roughness would be desirable.

ACKNOWLEDGMENTS

The authors thank Professor G. E. W. Bauer and Y. Asano for valuable discussions and Dr. R. Eder for critical reading of this manuscript. Also the authors thank the computer center, Institute for Molecular Science, Okazaki National Research Institutes for the use of the HITACHI M-680H and S-820/80 computers.

[1] P. Grünberg, R. Schreiber, Y. Pang, M. B. Brodsky, and H. Sowers, Phys. Rev. Lett. **57**, 2442 (1986).
[2] S. S. P. Parkin, Phys. Rev. Lett. **67**, 3598 (1991).
[3] M. N. Baibich, J. M. Broto, A. Fert, Nguyen Van Dau, F. Petroff, P. Etienne, G. Creuzet, A. Friederich, and J. Chazelas, Phys. Rev. Lett. **61**, 2472 (1988).
[4] D. H. Mosca, F. Petroff, A. Fert, P. A. Schroeder, W. P. Pratt, Jr., and R. Loloee, J. Magn. Magn. Mater. **94**, L1 (1991).
[5] S. S. P. Parkin, R. Bhadra, and K. P. Roche, Phys. Rev. Lett. **66**, 2152 (1991).
[6] T. Shinjo and H. Yamamoto, J. Phys. Soc. Jpn. **59**, 3061 (1990).
[7] Y. Saito and K. Inomata, Jpn. J. Appl. Phys. **30**, L1773 (1991); K. Inomata and Y. Saito, J. Magn. Magn. Mater. **126**, 425 (1993).
[8] N. Kataoka, K. Saito, and H. Fujimori, J. Magn. Magn. Mater. **121**, 383 (1993).
[9] H. Kubota, S. Ishio, and T. Miyazaki, J. Magn. Magn. Mater. **126**, 463 (1993).
[10] M. Jimbo, T. Kanda, S. Goto, S. Tsunashima, and S. Uchiyama, J. Magn. Magn. Mater. **126**, 422 (1993).
[11] A. Barthélémy, A. Fert, M. N. Baibich, S. Hadjoudj, F. Petroff, P. Etienne, R. Cabanel, S. Lequien, F. Nguyen Van Dau, and G. Creuzet, J. Appl. Phys. **67**, 5908 (1990).
[12] W. P. Pratt, Jr., S. F. Lee, J. M. Slaughter, R. Loloee, P. A. Schroeder, and J. Bass, Phys. Rev. Lett. **66**, 3060 (1991).
[13] S. F. Lee, W. P. Pratt, Jr., Q. Yang, P. Holody, R. Loloee, P. A. Schroeder, and J. Bass, J. Magn. Magn. Mater. **118**,

L1 (1993).
[14] W. P. Pratt, Jr., S. F. Lee, P. Holody, Q. Yang, R. Loloee, J. Bass, and P. A. Schroeder, J. Magn. Magn. Mater. **126**, 406 (1993).
[15] M. A. M. Gijs, S. K. J. Lenczowski, and J. B. Giesbers, Phys. Rev. Lett. **70**, 3343 (1993).
[16] G. E. W. Bauer, M. A. M. Gijs, S. K. J. Lenczowski, and J. B. Giesbers, J. Magn. Magn. Mater. **126**, 454 (1993).
[17] R. E. Camley and J. Barnaś, Phys. Rev. Lett. **63**, 664 (1989).
[18] P. M. Levy, S. Zhang, and A. Fert, Phys. Rev. Lett. **65**, 1643 (1990).
[19] D. M. Edwards, R. B. Muniz, and J. Mathon, IEEE Trans. Magn. **MAG-27**, 3548 (1991).
[20] A. Okiji, H. Nakanishi, K. Sakata, and H. Kasai, Jpn. J. Appl. Phys. **31**, L706 (1992).
[21] R. Q. Hood, L. M. Falicov, and D. R. Penn, Phys. Rev. B **49**, 368 (1994).
[22] A. Vedyaev, C. Cowache, N. Ryzhanova, and B. Dieny, J. Phys. Condens. Matter **5**, 8289 (1993).
[23] J. Inoue, A. Oguri, and S. Maekawa, J. Phys. Soc. Jpn. **60**, 376 (1991); J. Magn. Magn. Mater. **104-107**, 1883 (1992).
[24] J. Inoue, H. Itoh, and S. Maekawa, J. Phys. Soc. Jpn. **61**, 1149 (1992).
[25] J. Inoue and S. Maekawa, Prog. Theor. Phys. Suppl. **106**, 187 (1991).
[26] H. Itoh, J. Inoue, and S. Maekawa, Phys. Rev. B **47**, 5809 (1993).
[27] E. E. Fullerton, D. M. Kelly, J. Guimpell, and I. K. Schuller, Phys. Rev. Lett. **68**, 859 (1992).
[28] J. E. Mattson, C. H. Sowers, A. Berger, and S. D. Bader, Phys. Rev. Lett. **68**, 3252 (1992).
[29] P. Baumgart, B. A. Gurney, D. R. Wilhoit, T. Nguyen, B. Dieny, and V. S. Speriosu, J. Appl. Phys. **69**, 4792 (1991).
[30] S. S. P. Parkin, Phys. Rev. Lett. **71**, 1641 (1993).
[31] V. S. Speriosu, J. P. Nozieres, B. A. Gurney, B. Dieny, T. C. Huang, and H. Lefakis, Phys. Rev. B **47**, 11 579 (1993).
[32] J. Sakurai, M. Horie, S. Araki, H. Yamamoto, and T. Shinjo, J. Phys. Soc. Jpn. **60**, 2522 (1991).
[33] M. J. Conover, M. B. Brodsky, J. E. Mattson, C. H. Sowers, and S. D. Bader, J. Magn. Magn. Mater. **102**, L5 (1991).
[34] L. Piraux, A. Fert, P. A. Schroeder, R. Loloee, and P. Etienne, J. Magn. Magn. Mater. **110**, L247 (1992).
[35] J. Shi, S. S. P. Parkin, L. Xing, and M. B. Salamon, J. Magn. Magn. Mater. **125**, L251 (1993).
[36] F. Tsui, B. Chen, D. Barlett, R. Clarke, and C. Uher, Phys. Rev. Lett. **72**, 740 (1994).
[37] H. Sato, Y. Aoki, Y. Kobayashi, H. Yamamoto, and T. Shinjo, J. Magn. Magn. Mater. **126**, 410 (1993).
[38] S. S. P. Parkin, R. F. Marks, R. F. C. Farrow, G. R. Harp, Q. H. Lam, and R. J. Savoy, Phys. Rev. B **46**, 9262 (1992).
[39] H. Hasegawa, Phys. Rev. B **47**, 15 073 (1993); **47**, 15 080 (1993).
[40] J. L. Duvail, A. Fert, L. G. Pereira, and D. K. Lottis (unpublished).
[41] S. Zhang and P. M. Levy, J. Appl. Phys. **69**, 4786 (1991).
[42] H. E. Camblong, S. Zhang, and P. M. Levy, Phys. Rev. B **47**, 4735 (1993).
[43] T. Valet and A. Fert, Phys. Rev. B **48**, 7099 (1993).
[44] V. Ustinov, E. Kravtov, and V. Okutov (unpublished).
[45] P. B. Visscher, Phys. Rev. B **49**, 3907 (1994).
[46] G. E. W. Bauer, Phys. Rev. Lett. **69**, 1676 (1992).
[47] G. E. W. Bauer, A. Brataas, K. M. Schep, and P. J. Kelly, J. Appl. Phys. **75**, 6704 (1994).
[48] A. Brataas and G. E. W. Bauer, Europhys. Lett. **26**, 117 (1994).
[49] A. Oguri, Y. Asano, and S. Maekawa, J. Phys. Soc. Jpn. **61**, 2652 (1992).
[50] Y. Asano, A. Oguri, and S. Maekawa, Phys. Rev. B **48**, 6192 (1993).
[51] A part of the present study has been published by J. Inoue, H. Itoh, and S. Maekawa, J. Magn. Magn. Mater. **126**, 413 (1993).
[52] M. Tsukada, J. Phys. Soc. Jpn. **26**, 684 (1969).
[53] P. Soven, Phys. Rev. **156**, 809 (1967).
[54] B. Velicky, Phys. Rev. **184**, 614 (1969).
[55] K. Levin, B. Velicky, and H. Ehrenreich, Phys. Rev. B **2**, 1771 (1979).
[56] The Fermi velocity effect on the difference between ρ_{F} and ρ_{AF} has been argued by T. Oguchi, J. Magn. Magn. Mater. **126**, 519 (1993) in realistic band calculations.
[57] See, e.g., E. N. Economou, *Green's Functions in Quantum Physics* (Springer-Verlag, Berlin, 1983).